Petroleum Science 20 (2023) 2428–2441

Contents lists available at ScienceDirect

Petroleum Science

journal homepage: www.keaipublishing.com/en/journals/petroleum-science

Original Paper

# Effect of mechanical vibration process parameters on the cement plugs properties for abandoned wells

Hang-Ming Liu [a, b], Yang-Ye He [d, **], Ji-Fang Wan [c], Lin Chen [a, b], Xian-Zhong Yi [a, b, *], Yuan-Hua Zhou [a, b], Yu-Xian He [a, b], Xiang-Gui Ming [e], Lu Ren [e]

[a] Cooperative Innovation Center of Unconventional Oil and Gas, Yangtze University (Ministry of Education & Hubei Province), Wuhan, Hubei, 430100, China
[b] School of Mechanical Engineering, Yangtze University, Jingzhou, Hubei, 434023, China
[c] CNPC Engineering Technology R&D Company Limited, Beijing, 102206, China
[d] College of Safety and Ocean Engineering, China University of Petroleum-Beijing, Beijing, 102249, China
[e] Engineering Technology Research Institute, CNPC Bohai Drilling Engineering Co., Ltd., Tianjin, 300457, China

ARTICLE INFO

*Article history:*
Received 14 September 2022
Received in revised form
9 May 2023
Accepted 12 July 2023
Available online 13 July 2023

Edited by Jia-Jia Fei

*Keywords:*
Plugging and abandonment
Cement plug
Vibration
Mechanical properties
Microstructure

ABSTRACT

A high-quality plug of the abandoned wellbore is considered an essential technical aspect of the oil and gas well abandonment technology system. This paper presents a method of active mechanical excitation to enhance the quality of wellbore plug barriers. An indoor simulation platform is developed, and the effects of different combinations of vibration frequency, amplitude and duration on the properties of the wellbore plug cement material are investigated. It is observed that the optimal combination of excitation parameters occurs at a vibration frequency of 15 Hz, a vibration time of 6 min, and a vibration amplitude of 3 mm. Compared with the condition without the vibration process, the cementing strength, compressive strength, and tensile strength of wellbore cement plug with the optimal mechanical vibration process could increase by 51%, 38% and 20%, respectively, while the porosity decreases by 5%. As determined by scanning electron microscopy of the set cement's microstructure, mechanical vibration effectively eliminates internal porosity and improves the set cement's density. The optimal excitation parameters obtained from the test can guide the design of the vibration plugging tool. The designed vibration plugging tool is simulated in the near field. The cement plug cementation quality tester tests the vibrating and non-vibrating samples, and the cementation ratio is calculated. The test results show that the average cementation ratio of vibrating samples is 0.89375, and that of non-vibrating samples is 0.70625, and the cementation quality is improved by 27%. It is concluded that it not only provides essential data for the design of mechanical vibration plug apparatus, on-site vibration plugs, and the development of operational specifications for vibration plugs, but also provides solid engineering guidance.


## 1. Introduction

The oil/gas exploration and production wells are increasingly abandoned due to geological, engineering, and environmental reasons. Plugging and abandonment (P&A) operations prevent oil and gas leakages from hydrocarbon zones to various formations, underground freshwater resources, and the ground surface (Akbari and Taghavi, 2021). At the same time, the Environmental Protection Agency (EPA) estimates that abandoned oil and gas wells in the United States leaked about 263,000 tons of methane in 2019, which equals more than five coal-fired power plants (Whitehouse, 2021). Methane emission reduction has become one of the core objectives of global carbon neutrality. The most effective way to prevent methane emissions from abandoned wells is to store them in the well permanently. Fig. 1 shows the well structure and the possible leakage issues after plugging and abandonment. According to the Chinese disposal standard SY/T 6646 for abandoned wells (SY/T

* Corresponding author. Cooperative Innovation Center of Unconventional Oil and Gas, Yangtze University (Ministry of Education & Hubei Province), Wuhan, Hubei, 430100, China.
** Corresponding author. College of Safety and Ocean Engineering, China University of Petroleum-Beijing, Beijing, 102249, China.
*E-mail addresses:* yangyehe@cup.edu.cn (Y.-Y. He), zjrslhm@163.com (X.-Z. Yi).

https://doi.org/10.1016/j.petsci.2023.07.011

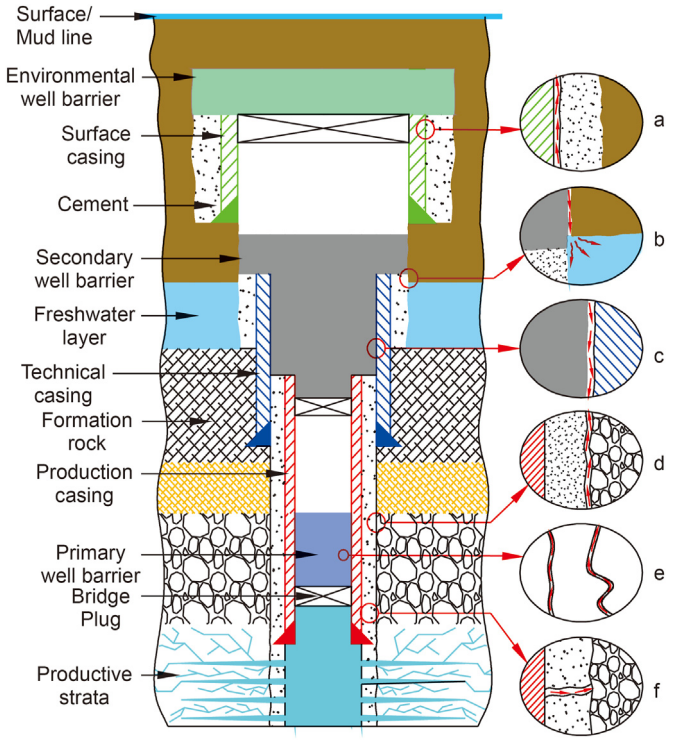


**Fig. 1.** Plug the wellbore structure after abandoned operation and possible leakage issues.

6646, 2017), the wellhead device must be removed first, followed by the cutting and recovery of the surface casing at a certain depth below the surface or seabed mud line and the restoration of topography. Finally, the plugging material is injected into the well to form a predetermined length of plugging barrier, and all essential layers are separated to prevent interfacial flow. According to statistics, well plugging and abandonment costs account for approximately 40%–44% of oil and gas well decommissioning expenses, which does not generate revenue (Gajdos et al., 2015). To minimize the leakage and reduce the cost of abandoning oil and gas wells, operators and research institutes worldwide seek practical solutions by utilizing reliable plug technology and relatively low-cost plug materials.

The most economical method for P&A disposal is to leave as much casing in the well as possible, and an additional low-cost and long-term plug barrier must be employed inside of the casing in the disposal well. With its low-cost and proven performance, Portland cement remains the most frequent plug material for disposal (Khalifeh et al., 2013; Trudel et al., 2019; Cui et al., 2021). Also, it has been reported that despite P&A disposal, certain oil wells in the Gulf of Mexico continue to leak. The principal sources of leakage are the cement plug-formation microring (Fig. 1(b)), the casing-cement plug microring (Fig. 1(c)), and cracks in the cement plug body (Fig. 1(e)) (Kaiser, 2017; Vrålstad et al., 2019; Kjøller et al., 2016; Walsh et al., 2013; Carey, 2013). In addition, abandoned wells may exhibit casing-cement ring cementation surface cracking (Fig. 1(a)), cement ring formation cementation surface cracking (Fig. 1(d)), and cement ring body cracking (Fig. 1(f)). If the quality of cement plugs in abandoned wells is inadequate, the fluid in the well will leak along the fracture under pressure, resulting in interlayer flow pollution of strata and freshwater resources, which poses potential threats to environmental and biological safety (Gajdos et al., 2015; Obodozie et al., 2016; Moeinikia et al., 2018; Bois et al., 2019). The normal bond strength between cement and casing plays a leading role in controlling interface fracture, interface debonding failure, and interface expansion failure (Lecampiona et al., 2013; Wang and Taleghani, 2014; Feng and Gray, 2017; Feng et al., 2017; Zhao et al., 2017). When the downhole liquid is under a high-pressure state, the fracture debonding height of the interface gradually decreases as the normal cementation strength of the interface increases. When the normal cementation strength of the interface increases from 0.25 to 2.0 MPa, the fracture debonding height of the interface decreases by 6.5 m (Jiang et al., 2020). Studies indicate that high normal cementation strength can inhibit the seepage of downhole high-pressure liquids and gases and effectively maintain the integrity of the plugging barriers of abandoned wells. Improving the cementing quality of abandoned well plugs is considered the main challenge of the disposal process.

The evaluation of the quality of cement plugs mainly focuses on macro and micro aspects. The main macro parameters are the mechanical properties of cement plugs, such as compressive strength, tensile strength and cementation strength. The microscopic properties are mainly reflected in the pore structure of the cement plug. Therefore, improving the quality of cement plugs is primarily achieved by enhancing their mechanical properties and microstructure, and the methods used mainly include chemical and physical processes. The chemical method to improve the performance of cement stone is to enhance the performance by adding different kinds of additives to the cement slurry. Among them, common cement slurry additives are polyurethane-silica, nano-$TiO_2$, graphene, rice husk ash, ethylene vinyl acetate, olivine microparticles, perlite particles, carboxylated styrene-butadiene latex powder and CSH-tartaric acid (Ma et al., 2022; Kumar et al., 2022; Kong et al., 2022; Huang et al., 2017; Lanka et al., 2022; Achang and Radonjic, 2021; Bageri et al., 2021; Zhao et al., 2022; Li H.Y. et al., 2022). The physical improvement method of cement paste performance is carried out by increasing the number of collisions between cement particles through vibration so that agglomerated cement particles can be separated, vibration can destroy bubbles, and the gap between the cement particles can be reduced so that the particles can occupy the position of the bubbles under the action of gravity, thus resulting in a dense vibration state. Cement is also a major component of concrete for civil and road engineering. Several studies have shown that the vibrating mixing process can improve the compressive strength, splitting compressive strength, tensile strength and density of concrete materials and effectively reduce micro-cracks and microporosity in concrete (Zheng et al., 2022; Cai et al., 2021; Xu and Li, 2021; Xiong et al., 2019, 2022; Zhang et al., 2020; Zhao et al., 2021). The frequency, amplitude and time of vibration are the key factors that affect the quality of concrete. Gao et al. (2019) chose two types of internal vibrators to reinforce fresh concrete. The effects of different vibration frequencies, vibration time and amplitude on fresh concrete were studied, respectively. It was found that for each mixture, the larger the vibration amplitude or the longer the vibration duration, the more serious the separation and the worse the long-term durability of the concrete.

According to the above literature review, the main plugging material of abandoned wells is cement. Many scholars have done a great deal of research on improving the mechanical properties of cement materials. There are mainly chemical methods and physical methods. The chemical method primarily uses various additives to modify cement materials. Physical methods are more widely used in civil engineering, road construction, etc., and the mechanical properties of concrete are improved by vibration mixing. However, there needs to be targeted research on the vibration plugging of abandoned oil and gas wells. The main purpose of this paper is to study the influence of different vibration parameter combinations on the mechanical properties of plugging cement plugs and obtain

the best combination of vibration parameters to guide the design of vibration plugging tools for abandoned wells and verify the reliability of vibration plugging tools through wellbore vibration plugging experiments. The main contents of this paper are as follows: (1) the influence of vibration parameters on the performance of cement paste was tested. (2) test the compressive strength, tensile strength, bonding strength, microstructure and porosity of the vibrated and non-vibrated samples to obtain the optimal vibration parameter combination. (3) using the vibration sealing tool designed according to the optimal vibration parameters to carry out the wellbore vibration sealing experiment and using the cement plug cementing quality tester to test the cementing rate of vibrating and non-vibrating samples. The research results can provide a reference for high-quality plugging of abandoned wells.

## 2. Experiment of the cement plugs with the mechanical vibration process

Section 2.1 presents the experiment procedure of the sample preparation. Section 2.2 gives the performance test of set cement.

### 2.1. Experiment procedure of the sample preparation

#### 2.1.1. Procedure and methodology of the experiment

The experimental apparatuses of the vibration platform for the cement plugs are shown in Fig. 2. It consists of a computer, a signal collector, a timer, a frequency converter, a vibrator, a vibration sensor, a magnetic counterweight and an experimental mould. The experimental device can provide different vibration environments for cement slurry and conduct experiments under various combinations of vibration parameters (vibration frequency, amplitude and vibration time). The timer controls the vibration duration, and the frequency converter regulates the vibration frequency. The magnetic counterweight adjusts the mass of the vibration platform to change its amplitude.

An orthogonal experiment is designed for the present work with three factors and five levels presented in Table 1 by employing the $L_{25}$ ($5^6$) orthogonal table (Zhang et al., 2022; Li X.J. et al., 2022). The factors of this experiment include vibration frequency, time and amplitude, and each factor is classified by five levels (namely 5, 10, 15, 20, 25 Hz; 2, 4, 6, 8, 10 min; 1, 2, 3, 4, 5 mm). The test factors and level numbers are assigned to the orthogonal table according to the corresponding positions. Table 1 presents the final 25 tests scheme in this orthogonal test.

The procedure and methodology of the experiment are given as follows:

(1) The cement slurry is prepared following API standards (API, 2019). The slurry is injected into the specimen preparation mould with a height of 150 mm in the square mould and 120 mm in the cylindrical mould.

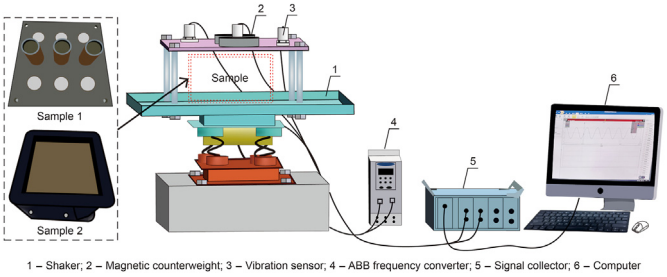


**Fig. 2.** Vibration platform for the cement plugs.

(2) The cement sample preparation mould is placed on the shaking table and fixed to the table utilizing a pressure plate and fastening bolts.
(3) Three vibration acceleration sensors are mounted at equal intervals on the surface of the plate along a diagonal direction. The input of the signal collector is plugged in, and the output of the signal collector is connected to the computer.
(4) After activating the power switch, the frequency converter sets the vibration frequency. The amplitude is adjusted using a magnetic counterweight, and a counter controls the vibration period. The vibration parameters (frequency, amplitude, and duration) are set according to the preset experimental protocol. After activating the vibration signal collector, the experiment begins.
(5) At the end of the experiment, the device is automatically stopped, the power is switched off, the experimental apparatus is dismantled, and the set cement preparation mould is wiped clean and placed under room temperature and pressure for a period of 24 h. After 24 h, the cement specimens are removed from the mould and placed under room temperature and pressure for another week.
(6) A rock coring water drill and rock cutter are used to divide each square cement block into three cylindrical specimens measuring 50 mm in diameter and 100 mm in height and three cylindrical specimens measuring 50 mm in diameter and 25 mm in height.
(7) The cut specimens are wiped clean, dried in a drying oven at 50 °C for 48 h, cooled to room temperature in a drying oven, and then examined.
(8)The strength is evaluated with an electronic universal testing machine, the microstructure with a scanning electron microscope, and the pore structure with a fully automatic mercury piezometer.

#### 2.1.2. Preparation of samples

The oil well cement (“Three Gorges” G grade), following the American Petroleum Institute (API) standards (API, 2019), is selected for this experiment. The chemical and mineralogical composition of the cement is given in Table 2.

Fig. 3 presents the preparation process of samples. The mixture of water and cement was thoroughly stirred with a small stirrer, and the prepared cement slurry density was 1.90 g/cm$^3$. The cement slurry is then poured into a cylindrical mould with an internal diameter of 50 mm and a height of 120 mm, leaving a 20 mm margin at the top of the mould, which is intended to carry the cement-casing for cement strength test (Fig. 3(a)). The slurry was poured into a square mould of 150 mm×150 mm×150 mm (Fig. 3(b)). After curing, each square cement block was cut into the cylindrical specimens for the compressive and tensile strength tests. Consequently, the three cylindrical specimens with a diameter of 50 mm and height of 100 mm are for testing the compressive strength, and the three cylindrical specimens with a diameter of 50 mm and height of 25 mm are for testing the tensile strength. This work uses the rock-coring water drill and rock cutter to cut the original square cement sample into cylindrical specimens. The remaining slices of set cement are utilized to examine the microscopic and pore structures.

The moulds containing cement slurry are weighed and recorded before being placed on a vibration table with a predetermined vibration frequency and time for vibration treatment. A comparison test is set up for the non-vibrated specimens, which are maintained under the same conditions as the vibrated specimens. The specimens are de-moulded after 24 h of standing, and the de-moulded specimens are conditioned at ambient temperature and pressure for one week.

**Table 1**
25 tests scheme in the orthogonal test.

| Scheme | (A) Vibration frequency, Hz | (B) Vibration time, min | (C) Vibration amplitude, mm |
|---|---|---|---|
| 1 | 5 | 2 | 1 |
| 2 | 5 | 4 | 3 |
| 3 | 5 | 6 | 5 |
| 4 | 5 | 8 | 2 |
| 5 | 5 | 10 | 4 |
| 6 | 10 | 2 | 5 |
| 7 | 10 | 4 | 2 |
| 8 | 10 | 6 | 4 |
| 9 | 10 | 8 | 1 |
| 10 | 10 | 10 | 3 |
| 11 | 15 | 2 | 4 |
| 12 | 15 | 4 | 1 |
| 13 | 15 | 6 | 3 |
| 14 | 15 | 8 | 5 |
| 15 | 15 | 10 | 2 |
| 16 | 20 | 2 | 3 |
| 17 | 20 | 4 | 5 |
| 18 | 20 | 6 | 2 |
| 19 | 20 | 8 | 4 |
| 20 | 20 | 10 | 1 |
| 21 | 25 | 2 | 2 |
| 22 | 25 | 4 | 4 |
| 23 | 25 | 6 | 1 |
| 24 | 25 | 8 | 3 |
| 25 | 25 | 10 | 5 |

**Table 2**
The mineral and chemical composition of oil well cement ("Three Gorges" G grade).

| Chemical composition, wt% | | | | | | Mineral composition, wt% | | |
|---|---|---|---|---|---|---|---|---|
| $SiO_2$ | $Al_2O_3$ | $Fe_2O_3$ | CaO | MgO | $SO_3$ | $C_3S$ | $C_2S$ | $C_4AF+2C_3A$ |
| 21.01 | 4.17 | 5.05 | 64.51 | 1.20 | 2.02 | 61.88 | 13.47 | 20.38 |

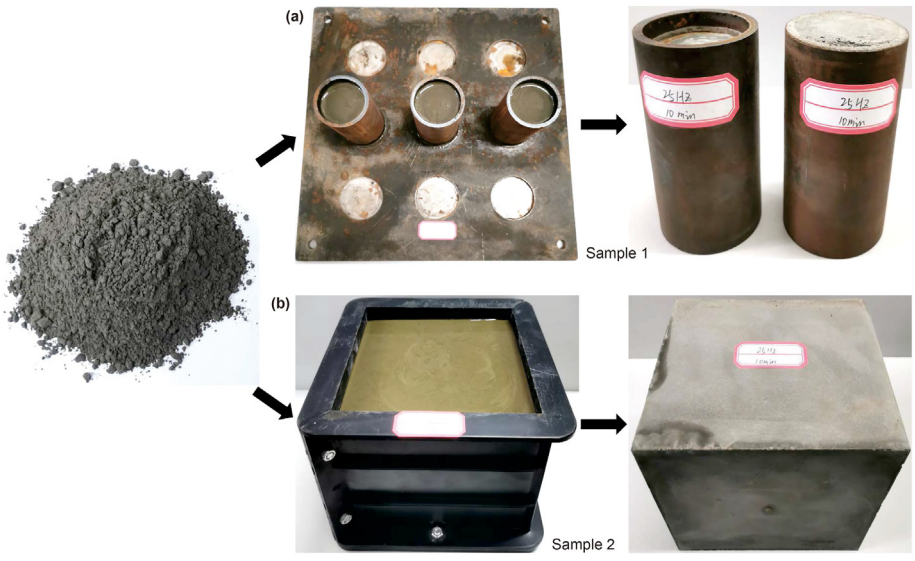


**Fig. 3.** Preparation of samples: (**a**) Sample 1: cementing strength test sample; and (**b**) Sample 2: preliminary samples of compressive strength and tensile strength tests.

## 2.2. Performance test of set cement

The uniaxial compressive strength, tensile strength, and cementing strength tests of the cement plug are presented in Sections 2.2.1–2.2.2. The porosity test of the cement plug is given in Section 2.2.3. Section 2.2.4 describes the scanning electron microscopy analysis of the cement plug.

### 2.2.1. Uniaxial compressive and tensile strength test

An electronic universal testing machine (Shimadzu Autograph type AG-I100) is used for the uniaxial compressive strength test. For the compressive strength of the cement test, the API standard requires cement blocks of 50 mm × 50 mm × 50 mm. However, experiments (James and Boukhelifa, 2008) have demonstrated that the compressive strength measured using square blocks will be approximately 15% higher than the actual value, and the cylindrical

cement with a height-to-diameter ratio greater than 1.8 is recommended for the compressive strength test. In this work, cylindrical specimens with a height of 100 mm and a diameter of 50 mm are tested with a loading rate of 0.6 mm/min according to ASTM C39/C39M-18 (2018) and GB/T 50266 (2013). Three samples are tested for each combination of vibration parameters in Table 1, and the total 75 results are averaged. The force and displacement relationship of the uniaxial compressive strength test is shown in Fig. 4. The progression of the compressive properties of set cement with increasing load can be separated into three stages, namely the OA stage for compaction, AB stage for linear elasticity, and BC stage for rupture of cement. The cement reaches its compressive limit at point B.

The uniaxial compressive strength of cement is calculated by (GB/T, 2013),

$$R_c = \frac{P}{A} \tag{1}$$

where $R_c$ represents the uniaxial compressive strength of cement (MPa), $P$ represents the peak force at the specimen failure (kN), and $A$ denotes the cross-sectional area of the specimen perpendicular to the loading direction ($mm^2$).

The method of measuring tensile strength is well-established in the standards for rock and concrete, but the API standard (API, 2019) has not yet given a standardised practice for the tensile strength testing of set cement. James and Boukhelifa (2008) selected a cylindrical specimen with a diameter twice the thickness and utilized the Brazilian test to measure the tensile strength of cement (Fig. 5), applying a loading rate of 0.6 mm/min until failure. The tensile strength ($\sigma_t$) of the specimen is calculated by:

$$\sigma_t = \left(\frac{0.636P}{DT}\right) \text{MPa} \tag{2}$$

where $P$ is the load at breakage (N), $D$ is the diameter of the specimen (mm), and $T$ is the thickness of the centre of the specimen (mm).

Three samples are tested for each combination of vibration parameters in Table 1, and the total 75 results are averaged. The force and displacement relationship of the tensile strength test is shown in Fig. 5. The development of the tensile properties of set cement with increasing load can be split into three stages, which include the OA stage for compaction, AB stage for linear elasticity, and BC stage for fracture failure.

### 2.2.2. Cementing strength test

A method of measuring the normal cementing strength is devised by substituting round tubing for the casing (Fig. 6(a)). This method sets cement immobilised, and the maximum pressure is determined by pressing the round tube against the shear cementing surface at a loading rate of 0.6 mm/min. Fig. 6(b) gives a photograph of the specimen after testing. The force and displacement relationship of the cementing strength test is shown in Fig. 6(c). The cementing between the plug and the tube in section OA is in the linear elastic phase. The maximum pressure measured at point A is the cementing force between the plug and the tube. In contrast, the cementing force in section AB is primarily frictional, so the contact area between the plug and the casing gradually decreases as the tube moves.

### 2.2.3. Porosity test

High-pressure mercury piezometric testing is performed using a Micromeritics AutoPore V 9600 fully automatic mercury piezometer at a maximum pressure of 600 MPa with a pore diameter range of 0.003–950 μm. The fundamental principle of the mercury-pressure method for characterisation of set cement pore throats is that the pore throat can be filled with a non-wetting fluid under pressure, and the pore throat radius can be calculated using capillary theory as the mercury is pressed into the pore throat (Delage, 2010; Han et al., 2022; Liu et al., 2022). The pore radius is given by (Washburn, 1921):

$$r = \frac{-2\sigma\cos\theta}{P} \tag{3}$$

where $r$ is the pore radius, $\sigma$ is the surface tension of the mercury, taken as 0.485 N/m, $\theta$ is the contact angle between the mercury and the solid material, taken as 130°, and $P$ is the applied pressure.

Before the high-pressure mercury test, the square cement sample with a volumetric surface of 1 $cm^3$ is polished. The choice of drying temperature is of great importance here. For materials such as set cement, mortar blocks, concrete, etc., drying at temperatures exceeding 100 °C will cause the water of crystallisation to escape and the original mineral lattice to be destroyed, resulting in a different compound. Therefore, the samples are dried at 55 °C for 48 h and then cooled to room temperature in a desiccator before testing.

### 2.2.4. Scanning electron microscopy (SEM) analysis

The set cement microstructure is analysed using JEOL's JSM-IT300A analytical scanning electron microscope. The cement specimens of 0.5 $cm^3$ in size are surface treated and dried before being sputtered for 2 min with a HITACHI E−1010 ion sputtering equipment to obtain a 10 nm thick gold film. The metallic film on the specimen's surface enhances the picture's quality.

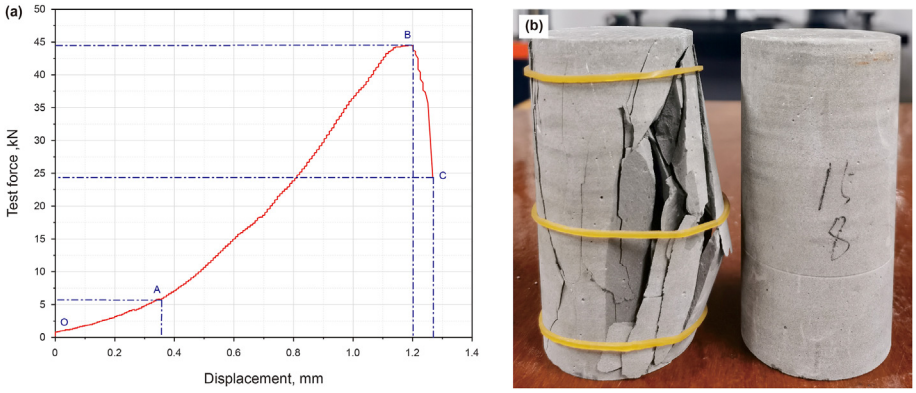


**Fig. 4.** Results of the uniaxial compressive strength test: (**a**) the curve of force and displacement; and (**b**) samples before and after the compressive strength test.

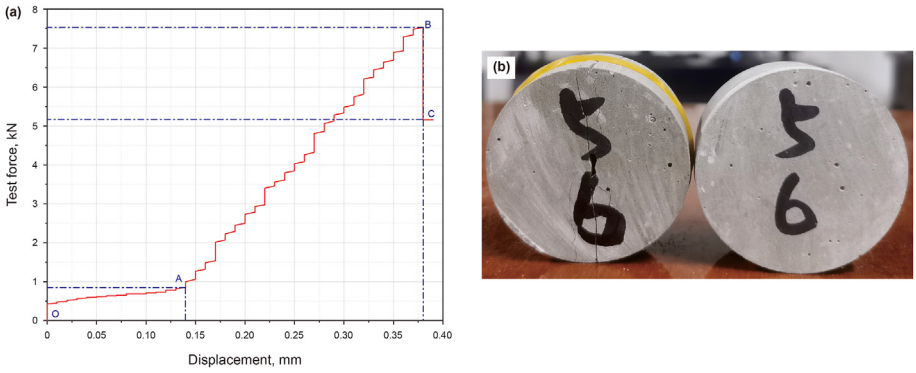


**Fig. 5.** Results of a tensile strength test: (**a**) the curve of force and displacement; and (**b**) samples before and after the tensile strength test.

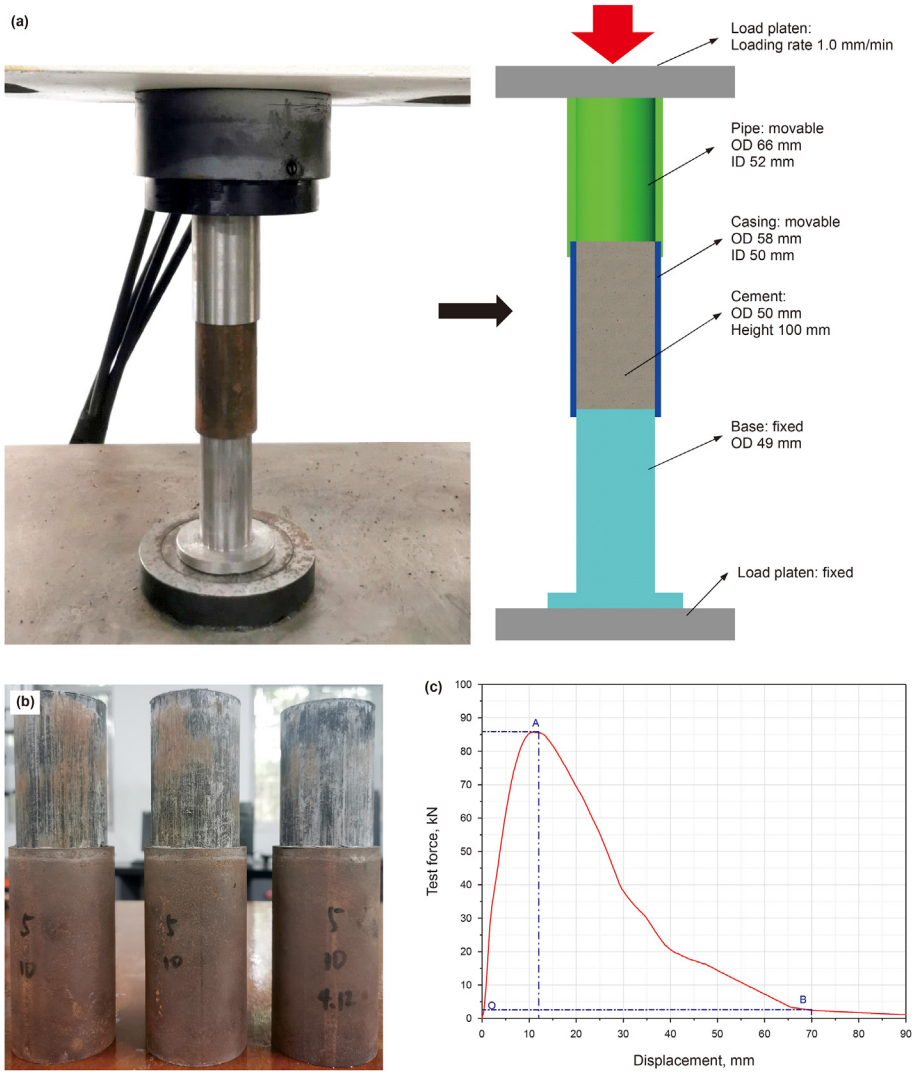


**Fig. 6.** Results of a cementation strength test: (**a**) the device of cementation strength test; (**b**) samples after the cementation strength test; and (**c**) the curve of force and displacement.

## 3. Results and discussions

Section 3.1 shows the mechanism of vibration improvement of plug set cement. Section 3.2 presents the effect of vibration parameters on plug mechanical properties of set cement. Section 3.3 shows the pore structure of the cement plug. Section 3.4 shows the microstructure of the cement plug. Section 3.5 presents the simulation experiment of vibration plugging of abandoned wells.

### 3.1. Mechanism of vibration improvement of plug set cement

The application of mechanical vibration considerably enhances the cement's mechanical properties, pores, and microstructure during the hydration phase. This is because the stress waves generated by the mechanical vibration on the cement particles are subjected to shear forces, which are vertical stresses varying in size and direction. The shear stress primarily influences the induction and setting phases of the cement hydration processes. This is the most critical period of cement hydration, with its mechanism described as follows.

During the induction period, the main mineral in the oil well cement, $C_3S$, undergoes rapid chemical reactions. $Ca(OH)_2$ and C–S–H nuclei begin to form, and the $Ca^{2+}$ ion concentration reaches supersaturation. Providing mechanical vibration at this moment can facilitate the hydration reaction of $C_3S$ with water and shorten the induction period of the cement.

During the condensation phase, $Ca(OH)_2$ and C–S–H nuclei rapidly hydrate and form C–S–H gels and $Ca(OH)_2$ crystals. At this point, large amounts of $Ca(OH)_2$ precipitate out of the solution to form crystals, and large quantities of C–S–H gels form and fill the entire hydration system. Some of the hydration products are adsorbed or deposited on the surface of the C–S–H gel, influencing the rate of the C–S–H hydration reaction (Ding et al., 2007; Panesar and Shindman, 2012). The deposition and adsorption of hydration products and cement mineral particles are disrupted by mechanical vibration, leading to the increased contact area between the C–S–H gel and the surrounding water body, early hydration of the cement, and the increased hydration efficiency of C–S–H. The mechanical vibration process increases the cement's early strength, reduces the cement's porosity, and enhances the compactness of cement.

In addition, the newly injected slurry may contain agglomerations of cement particles, air bubbles, and voids, which can influence its compatibility and strength. This is because the hydration of the cement occurs only on the surface of the cement particles. If the cement particles agglomerate, the area of hydration is reduced, resulting in a less intense hydration product. Vibration increases the number of collisions between cement particles, separates agglomerated cement particles, and at the same time destroys the air bubbles, reduces the gap between cement particles, and allows the particles to occupy the position of the air bubbles by gravity, resulting in a vibrationally dense state. Fig. 7 compares the mud state before and after vibration. After vibration, the internal air bubbles are broken and discharged, and the released air bubbles are gathered on the surface of the mud to form four foam clusters. Simultaneously, the vibration makes the slurry particles more evenly distributed, and the gap between the particles becomes smaller, resulting in water seepage and the sinking of the particles to achieve a dense state.

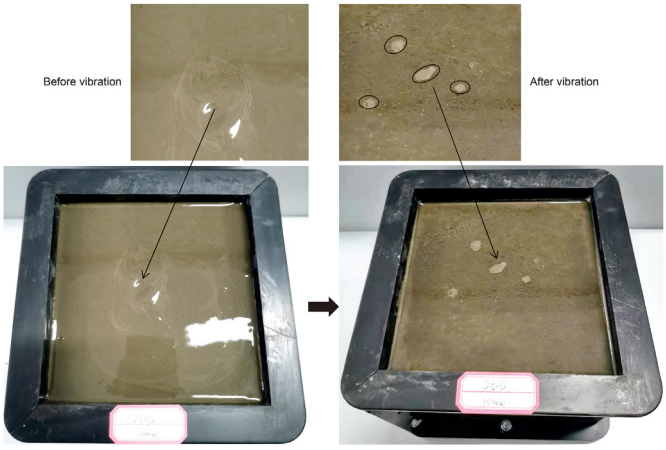


**Fig. 7.** Macroscopic comparison of cement slurry before and after vibration.

Vibration can destroy the bubbles in the cement slurry, separate the agglomerated cement particles, promote the cement's hydration reaction, and increase the cement's early strength.

### 3.2. Effect of vibration parameters on plug mechanical properties of set cement

The cementitious strength, compressive strength, and tensile strength of the cement samples conducted under various operating conditions are presented in Table 3, in which Sample 0 and Samples 1–25 represent the samples without vibration and under different vibration parameter combinations, respectively. In this work, the range analysis method is utilized to assess the data of orthogonal test results. Assume that $X$ and $Y$ are two distinct influencing factors in the experiment; $X_i$ represents the value of factor $X$ at the $i$ level, $i = 1,2, \ldots, n$; $M_{ij}$ represents the $i$ level of factor $j$, $i = 1,2, \ldots, n$; $j = X, Y, \ldots$; Carry out $n$ trials under $M_{ij}$ to obtain $n$ trial results $N_k$, $k = 1, 2, \ldots, n$.

$$K_{ij} = \frac{1}{n}\sum_{k=1}^{n} N_k - \overline{N} \tag{4}$$

where $K_{ij}$ is the average value of factor $j$ at $i$ level; $n$ is the number of trials for factor $j$ at level $i$; $N_k$ is the $k$-th test value; and $\overline{N}$ is the average of all test results.

The sensitivity of the range analysis factor is evaluated using the range $R$, and the calculation formula is as follows:

$$R = \mathrm{Max}\{K_{1j}, K_{2j}, \cdots K_{nj}\} - \mathrm{Min}\{K_{1j}, K_{2j}, \cdots K_{nj}\} \tag{5}$$

The greater the range $R$ is, the greater the influence of the level change of the factor on the test index, that is, the greater the factor's sensitivity. On the contrary, the smaller the range of $R$, the smaller the sensitivity of the factors.

The impact of different vibration parameters (frequency, time, and amplitude) on the growth of cementing strength, compressive strength, and tensile strength of samples in comparison to samples without vibration is presented in Fig. 8. The mechanical properties of set cement after mechanical vibration treatment are significantly enhanced compared to those without vibration.

To obtain the degree of influence of each vibration factor on the mechanical properties of set cement, the results of the orthogonal tests are subjected to a polar difference analysis, as presented in Table 4.

It can be seen in Table 4 that the range $R$ of the differences of the vibration frequency, vibration time, and vibration amplitude is as follows: vibration frequency is more significant than vibration amplitude, while vibration amplitude is greater than vibration time.

According to the orthogonal test results, the effects of vibration frequency, vibration time, and vibration amplitude on the mechanical properties of set cement are as follows: vibration frequency is more significant than vibration amplitude. In contrast, vibration amplitude is greater than vibration time.

The optimum level for this test is A3B3C3 (Sample 13). This means that the most significant increase in strength is achieved at a vibration frequency of 15 Hz, a vibration time of 6 min, and a vibration amplitude of 3 mm, with a 51% increase in cementitious strength, a 38% increase in compressive strength, and a 20% increase in tensile strength.

**Table 3**
Orthogonal test protocol and results.

| Sample No. | Vibration frequency (A), Hz | Vibration time (B), min | Vibration amplitude (C), mm | Cementitious strength, MPa | Compressive strength, MPa | Tensile strength, MPa |
|---|---|---|---|---|---|---|
| 0 | 0 | 0 | 0 | 5.51 | 22.75 | 3.83 |
| 1 | 5 | 2 | 1 | 6.25 | 25.01 | 4.12 |
| 2 | 5 | 4 | 3 | 7.11 | 26.42 | 4.15 |
| 3 | 5 | 6 | 5 | 6.59 | 25.51 | 4.21 |
| 4 | 5 | 8 | 2 | 7.32 | 28.90 | 4.37 |
| 5 | 5 | 10 | 4 | 6.19 | 24.30 | 4.04 |
| 6 | 10 | 2 | 5 | 6.82 | 27.32 | 4.15 |
| 7 | 10 | 4 | 2 | 7.79 | 29.42 | 4.49 |
| 8 | 10 | 6 | 4 | 6.94 | 27.21 | 4.35 |
| 9 | 10 | 8 | 1 | 7.05 | 28.412 | 4.39 |
| 10 | 10 | 10 | 3 | 7.31 | 29.42 | 4.42 |
| 11 | 15 | 2 | 4 | 6.81 | 27.99 | 4.32 |
| 12 | 15 | 4 | 1 | 7.89 | 29.29 | 4.46 |
| 13 | 15 | 6 | 3 | 8.34 | 31.31 | 4.58 |
| 14 | 15 | 8 | 5 | 7.40 | 27.11 | 4.45 |
| 15 | 15 | 10 | 2 | 7.35 | 29.21 | 4.49 |
| 16 | 20 | 2 | 3 | 7.51 | 29.21 | 4.51 |
| 17 | 20 | 4 | 5 | 6.68 | 26.74 | 4.29 |
| 18 | 20 | 6 | 2 | 7.86 | 29.54 | 4.53 |
| 19 | 20 | 8 | 4 | 6.59 | 26.01 | 4.25 |
| 20 | 20 | 10 | 1 | 8.01 | 28.54 | 4.47 |
| 21 | 25 | 2 | 2 | 7.71 | 29.12 | 4.50 |
| 22 | 25 | 4 | 4 | 7.15 | 27.11 | 4.35 |
| 23 | 25 | 6 | 1 | 7.92 | 29.81 | 4.52 |
| 24 | 25 | 8 | 3 | 7.95 | 30.25 | 4.54 |
| 25 | 25 | 10 | 5 | 6.17 | 24.21 | 4.31 |

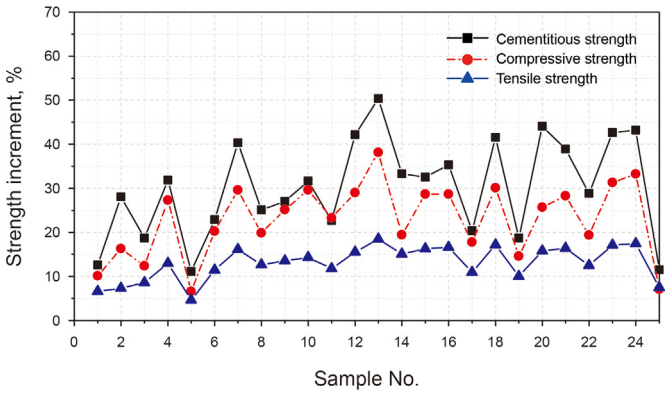


**Fig. 8.** Cementitious, compressive and tensile strengths increments of 25 samples after the mechanical vibration treatment.

A1B5C4 (Sample 5) is considered as the smallest increment in strengths achieved at a vibration frequency of 5 Hz, a vibration time of 10 min, and a vibration amplitude of 4 mm, namely with 10.1%, 6% and 4.8% increasements in the cementitious, compressive, and tensile strengths respectively.

A sensitivity study is carried out to investigate further the effects of vibration frequency, vibration time, and vibration amplitude on the mechanical properties of set cement by varying vibration parameters within a specific range (5–25 Hz, 2–10 min, and 1–5 mm), utilizing the vibration parameters at the optimal level of Sample 13 (15 Hz, 6 min, and 3 mm) as a reference. The test protocol is given in Table 5.

(1) Effect of vibration frequency on mechanical properties of set cement

Fig. 9 presents the cementitious, compressive, and tensile strength increments related to the vibration frequencies of 5, 10, 15, 20, and 25 Hz, respectively, after the mechanical vibration treatments compared with the strengths without vibration. The strength of set cement after vibration is greater than that of set cement without vibration. As the vibration frequency increases, the set cement's cementitious and tensile strengths increase gradually. At the same time, the compressive strength reduces slightly at 10 Hz. At a vibration frequency of 15 Hz, the cementitious, compressive and tensile strength reach their maximum values. When the vibration frequency exceeds 15 Hz, the cementitious, compressive and tensile strength increments in set cement gradually decrease.

(2) Effect of vibration time on the mechanical properties of set cement

Fig. 10 presents the cementitious, compressive, and tensile strength increments related to the vibration time of 2, 4, 6, 8, and 10 min, respectively, after the mechanical vibration treatments compared with the values without vibration. As

**Table 4**
Range analysis of orthogonal test results.

| | Range *R* | | |
|---|---|---|---|
| | Vibration frequency | Vibration time | Vibration amplitude |
| Cementitious strength | 0.95 | 0.43 | 0.91 |
| Compressive strength | 3.22 | 0.98 | 3.05 |
| Tensile strength | 0.29 | 0.10 | 0.21 |

**Table 5**
One-factor impact test protocol.

| Study factors | Vibration frequency, Hz | Vibration time, min | Vibration amplitude, mm |
|---|---|---|---|
| Vibration frequency | 5,10,15,20,25 | 6 | 3 |
| Vibration time | 15 | 2,4,6,8,10 | 3 |
| Vibration amplitude | 15 | 6 | 1,2,3,4,5 |

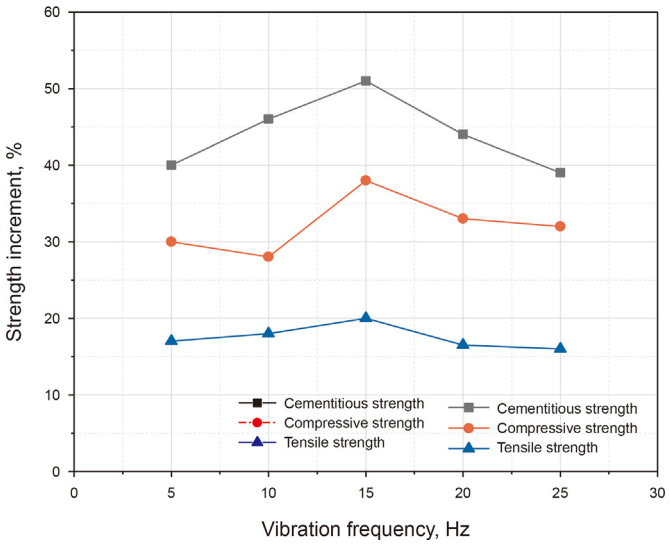


**Fig. 9.** Strength increment versus vibration frequency of mechanical vibration treatment.

the vibration time increases, the parameter values of the set cement rise gradually and then decrease. After 6 min of vibration, the highest growth in set cement strength is obtained. When the vibration duration exceeds 6 min, the increase in set cement strength decreases. Increasing the vibration time subsequently has minimal effect on the set cement strength, which is not significantly altered by consecutive increases.

(3) Effect of vibration amplitude on the mechanical properties of set cement

Fig. 11 presents the cementitious, compressive, and tensile strength increments related to the vibration amplitudes of 1, 2, 3, 4, and 5 mm, respectively, after the mechanical vibration treatments compared with the strengths without vibration. As the vibration amplitude increases, the three strengths of the set cement increase gradually and then decrease. With the vibration amplitude of 3 mm, the maximum increments in set cement strengths are reached.

After mechanical vibration treatment, the cementitious, compressive, and tensile strengths of the set cement are superior to the properties of set cement without vibration, as shown in Figs. 9–12. The optimal combination of vibration parameters obtained from the tests is a vibration frequency of 15 Hz, vibration time of 6 min, and vibration amplitude of 3 mm, which increases the cementitious strength by 51%, the compressive strength by 38%, and the tensile strength by 20% compared to specimens without vibration. When the vibration parameters are too small during mechanical vibration treatment, the air bubbles in the cement slurry cannot be broken and released completely; when the vibration parameters are excessively high, the cement slurry separates and becomes segregated and waterlogged.

### 3.3. Pore structure of set cement

In site, the upward permeation of high-pressure fluids and gases may occur, passing the pores of the plug set cement. Therefore, a high-pressure mercury intrusion test is used to analyse the pore characteristics of the plug set cement. From the effect analyses of the vibration parameters of mechanical vibration treatment on the mechanical properties of set cement, Samples 13 and 5 have the

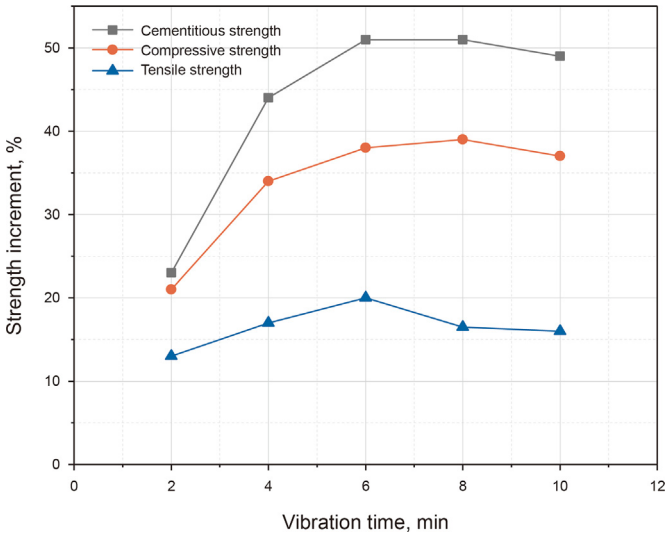


**Fig. 10.** Strength increment versus vibration time of mechanical vibration treatment.

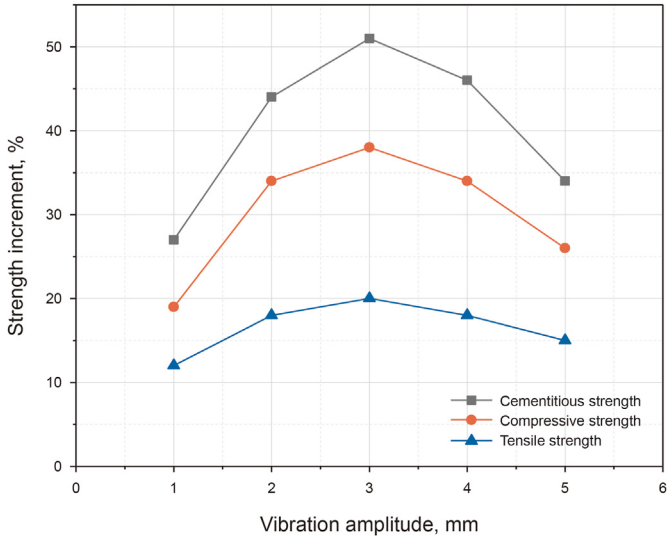


**Fig. 11.** Strength increment versus vibration amplitude of mechanical vibration treatment.

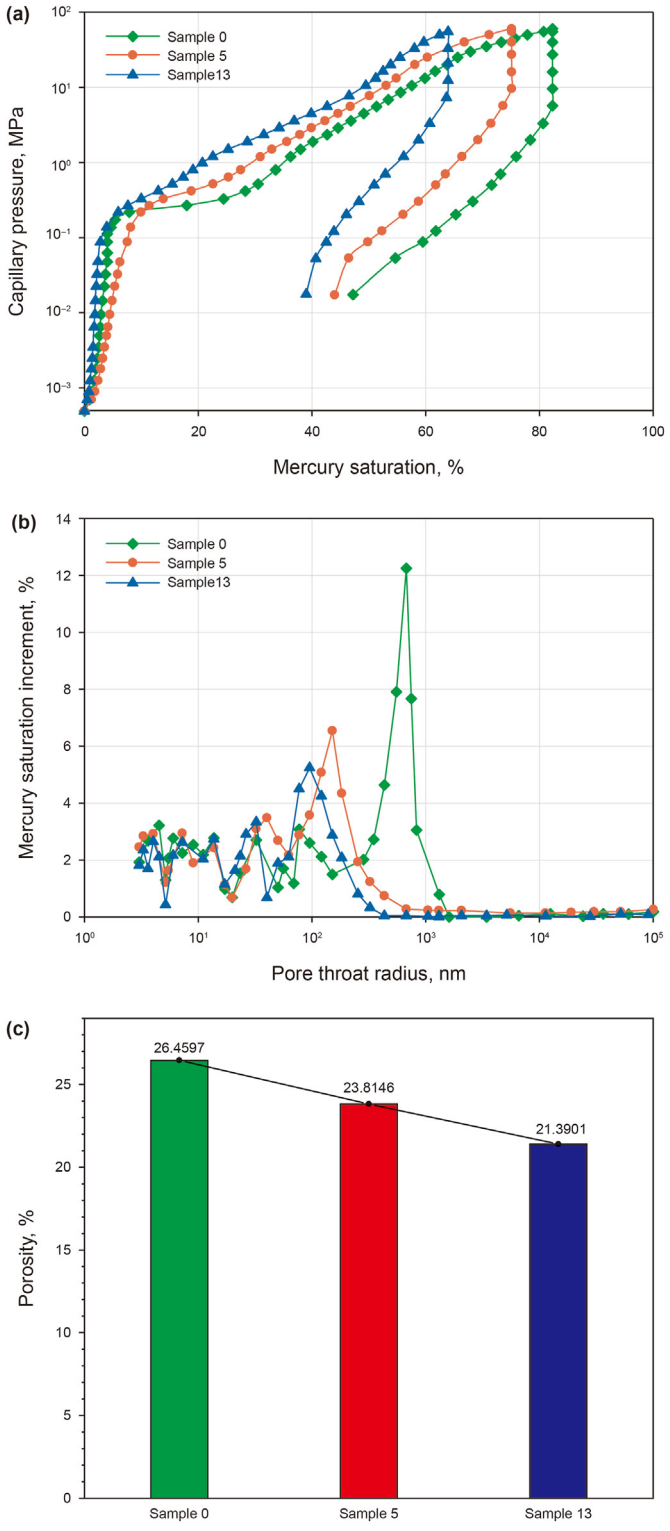


**Fig. 12.** (**a**) The capillary pressure versus mercury saturation; (**b**) mercury saturation increment versus pore throat radius of the set cement measured by high-pressure mercury intrusion test; and (**c**) comparison of porosity of three set cement samples.

highest and smallest mechanical properties increments of set cement, respectively. Also, both samples are superior to Sample 0 without vibration. The pore characteristics of three samples (Samples 0, 5 and 13) in the above typical cases are given in Table 6.

Fig. 12 presents the capillary pressure related to the mercury saturation and mercury saturation increment related to the pore throat radius of set cement of three samples measured by high-pressure mercury intrusion test. The capillary pressure associated with the mercury saturation profile of the plug set cement is characterised in Fig. 12(a). The mercury saturation is very low with the lower capillary pressure in the mercury feed phase as the sample suffers a low driving pressure, and subsequently, the mercury saturation increases as the capillary pressure increases. When the capillary pressure drops, mercury saturation stays constant and then decreases. During the same high-pressure mercury intrusion test, Samples 0, 5, and 13 have large, middle, and small mercury saturation, respectively.

The capillary pressure profiles of the samples are converted into pore throat diameter according to Washburn's equation (Fig. 12(b)). The graph depicts the discrepancy between the three samples' pore throat size distribution and permeability. Sample 0 possesses the more extensive pore throat radius range, the enormous pore volume, and the most prominent peak of pore throat radius distribution with peaks in the range of $5.5\times10^{2}$–$1\times10^{3}$ nm, corresponding to the highest porosity and permeability. Sample 5 has a narrower pore throat radius range with peaks in the 90–130 nm range, indicating smaller porosity and permeability. The pore throat radius range of Sample 13 is the narrowest, with peaks between 92 and 108 nm, corresponding to the lowest porosity and permeability. As the mechanical vibration treatment effect increases, the pore throat radius distribution becomes narrower with a smaller value of the principal peak. The change in porosity size of the three samples is shown in Fig. 12(c).

The porosity of cement samples with the best combination of vibration parameters was the lowest, 19.16% lower than that of the non-vibrating cement samples. Vibration can improve the ability of plugging cement plugs in abandoned wells to resist the seepage of high-pressure fluids and gas in the bottom of the well.

### 3.4. Microstructure of set cement

The accumulation of microscopic damage primarily causes macroscopic damage in plug-set cement, and the material's microstructure dictates its macroscopic properties (Wang et al., 2010). The process of hydration of cement, whereby hydration products continuously replenish the space occupied by cement and water, is a process in which the internal pores of set cement are predominately porous. Set cement damage begins with initial defects or faults before loading the set cement. When the set cement is loaded, the internal micro-cracks or pores become concentrated and expand, resulting in tracking in the cement. This leads to micro-annular gaps forming in the cement-casing joint. Therefore, the micro-structure of set cement with and without vibration is compared using scanning electron microscopy based mainly on the pores and cracks.

Note that when observing the surface of the specimen, the largest pores are sought for magnification in the following processes: Sample 0, Sample 13, and Sample 5.

As cement paste is a non-conductive material, to obtain high-quality images, it is necessary to spray gold on the surface of cement paste samples to increase its conductivity. Considering the cost of the experiment, we selected three samples (Sample 0, Sample 13 and Sample 5) for testing. These three samples represent the sample with no vibration (Sample 0), the sample with the best combination of vibration parameters (Sample 13) and the sample with the worst variety of vibration parameters (Sample 5). Amongst them, by comparing Sample 0 and Sample 5, we can explain the microstructure difference between vibrating and non-vibrating samples. By comparing Sample 13 and Sample 5, the microstructure difference between samples with the best and worst vibration parameters can be illustrated.

**Table 6**
Pore characteristic parameters of set cement.

| Sample No. | Threshold pressure, psia | Median pressure, MPa | Sorting factor | Skewness | Maximum orifice radius, nm | Median radius, nm | Maximum mercury feed saturation, % | Porosity, % |
|---|---|---|---|---|---|---|---|---|
| 0 | 0.79 | 5.58 | 3.108 | 0.241 | 1717.74 | 16.19 | 82.31 | 26.4597 |
| 5 | 1.74 | 7.72 | 3.795 | −0.135 | 338.26 | 10.55 | 75.14 | 23.8146 |
| 13 | 3.30 | 11.44 | 2.788 | 0.004 | 216.23 | 7.99 | 63.95 | 21.3901 |

Fig. 13 presents the micro-structure of the set cement samples at a magnification of 500×. Fig. 13(a) shows the microstructure of the set cement sample without vibration (Sample 0) with a wide and deep pore, micro-cracks extending outwards from the pore, a large number of tiny pores, a loose micro-structure, and poor densities. Fig. 13(b) depicts the micro-structure of the set cement for the vibration parameter combination of frequency, time and amplitude of 15 Hz, 6 min and 3 mm, respectively (Sample 13), which reveals a solid, dense microstructure with no microscopic cracks or pores. Fig. 13(c) depicts the micro-structure of the set cement for the vibration parameter combination of frequency, time and amplitude of 5 Hz, 10 min and 4 mm, respectively (Sample 5), in which one obvious pore is on the surface, no cracks are found, and the microstructure is relatively dense.

Through the comparative observation of vibrating and non-vibrating samples, the number of pores and cracks in the vibrating sample is much less than that in the non-vibrating sample. No cracks and pores are found in the sample obtained under the optimal vibration parameters, showing a compact microstructure.

### 3.5. Simulation experiment of vibration plugging of abandoned wells

The cement plugs of plugging abandoned wells isolate oil and gas layers, prevent interlayer channelling and protect freshwater layers. The cementing quality between the casing and cement plug determines the plugging quality of abandoned wells, while for permanently abandoned wells, the requirement is higher. In Section 2, the influence of vibration on the performance of cement paste is studied, and the bonding force between steel pipe and cement is tested. The results show that the vibrated samples' bonding force is improved compared to that of the non-vibrated samples. Under the optimum combination of vibration parameters, the bonding strength of the sample increased by 51%. To further verify that the vibration plugging method can effectively improve the cementing quality between casing and cement plug, a simulation experiment of vibration plugging of abandoned wells is designed. The experimental process and device are shown in Fig. 14.

In experiment (a), the dynamic characteristics of the vibration plugging tool were tested. The experiment aims to obtain the relationship between the displacement of the mud pump, the vibration frequency and the amplitude of the vibration plugging tool. When the density of cement slurry is 1.9 g/cm$^3$, and the displacement of the mud pump is 30 m$^3$/h, the amplitude of the vibration plugging tool is 3.05 mm, and the vibration frequency is 15.2 Hz. This result is close to the optimal vibration frequency and amplitude obtained in Section 2 of this paper. The optimum vibration frequency is 15 Hz and the optimum vibration amplitude is 3 mm. Therefore, to further verify the accuracy of the experimental results, the displacement of the mud pump is 30 m$^3$/h in the vibration plugging simulation experiment.

In experiment (b), the simulation experiment of vibration plugging of abandoned wells was carried out. Experimental process: the cement slurry is thoroughly stirred by a blender, and the density of the cement slurry is adjusted to 1.9 g/cm$^3$. The cement slurry is delivered to the mud tank through the surface screw pump, and the outlet of the mud tank is connected to the inlet of the mud pump. The engine group drives the mud pump, and the displacement of the mud pump is controlled by adjusting the engine speed. The displacement of the mud pump is held at 30 m$^3$/h. The mud pump transports the cement slurry to the vibrating plugging tool, which vibrates under the drive of the cement slurry, and the vibrated cement slurry enters the casing to form plugging. At the same time, a comparative test was conducted. In contrast experiment, the density of cement slurry was 1.9 g/cm$^3$, and the casing was injected with a mud pump. During the whole injection process, no vibration plugging tool was used, and no vibration occurred.

Experiment (c) tested the bonding quality between the casing and the cement plug. In the plugging of abandoned wells, the cement plug is injected into the casing, but the traditional cementing quality tester measures the cementing quality in the casing. Therefore, the traditional cementing quality tester can't detect the quality of cement plugs. To solve this problem, a six-sector cement plug quality tester is designed based on the principle of sector cement logging (Yu et al., 2014). The instrument can emit ultrasonic signals from the outer wall of the casing and measure the cementing quality between the inner wall of the casing and the cement plug. Because the tester's ultrasonic signal is easily lost and scattered in the air, testing in water can reduce the attenuation of ultrasonic waves. Therefore, the solidified casing with a sealing plug is put into the water tank, and the cementing quality of the sealing plug and the inner wall of the casing is

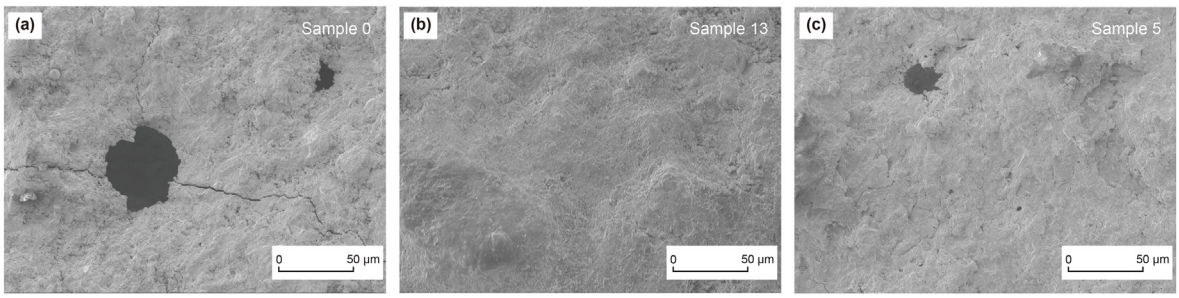


**Fig. 13.** Microscopic morphology of the specimen.

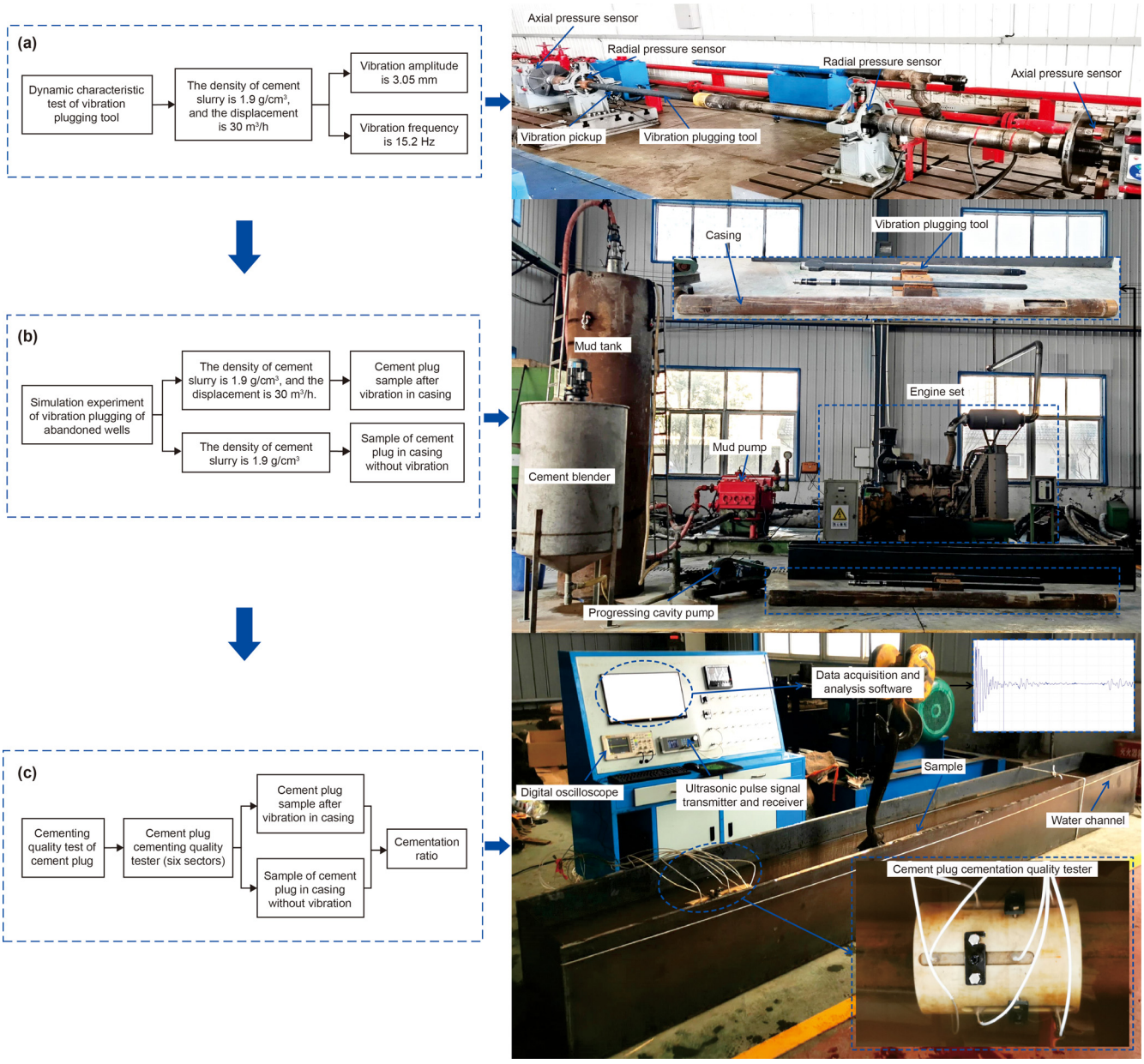


**Fig. 14.** Flow chart and device diagram of vibration plugging simulation experiment: (**a**) the test of dynamic characteristics of vibration plugging tool; (**b**) the simulation experiment of vibration plugging of abandoned wells; and (**c**) the test of bonding quality between casing and cement plug.

detected by the cement plug cementing quality tester. Six samples were tested in the experiment; three were vibrated, and three were not. According to the cementing quality evaluation method (SY/T 6592-2016), the acoustic attenuation rate is converted into cementing ratio, and the cementing quality between the plugging and casing inner wall is evaluated by cementing ratio. The cementing ratio refers to the percentage of acoustic attenuation rate after deducting the influence of the casing to the current cementing section where the cement sheath is completely cemented.

Fig. 15 reflects the change in cementing ratio related to depth between vibrating and non-vibrating samples. The evaluation method of cementing quality (SY/T 6592-2016) gives an evaluation index of cementing quality. When the cementation ratio is greater than or equal to 0.8, it is considered that the cementation quality of cement is excellent. When the cementation ratio is less than 0.5, the cementation quality of cement is considered unqualified. A cement plug cementing quality tester measured the cementing quality of vibrating and non-vibrating samples. The average cementation ratio between the vibrating plug to the inner surface of the casing is 0.89375. The average cementation rate of non-vibrated samples is 0.70625. The post-vibration cementing ratio is greater than 0.8, and the cementing quality is good. Compared with the non-vibrated sample, the cement ratio of the vibrated sample increased by 27%.

Through the vibration plugging tool, the vibration plugging simulation experiment of abandoned wells is carried out, which again proves that vibration can improve the plugging quality of cement plugs.

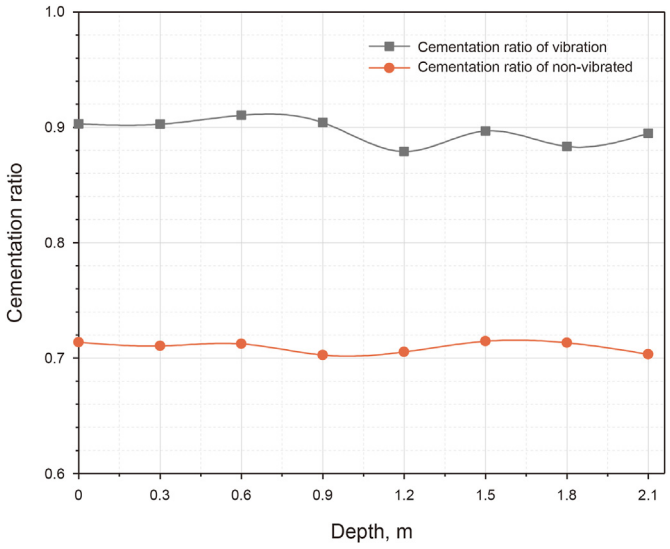


**Fig. 15.** Cementation ratio of vibrating and non-vibrating cement plug samples.

## 4. Conclusion

In this paper, the influence of vibration on the performance of cement plug and the simulation experiment of wellbore vibration plugging are carried out. In the experiment, the cement material is the same, and the curing and testing conditions of the specimens are the same. The influence of mechanical vibration parameters on the mechanical properties, pore structure and microstructure of abandoned well cement plugs was studied by experiments. The optimal combination of vibration parameters is determined, and guidance on the design of vibration plugging tools is provided. The experimental results show that mechanical vibration can effectively improve the mechanical properties of cement plugs and the cementing quality between casing and cement plugs. The main conclusions of this study are as follows:

(1) The experimental results of the influence of vibration on the properties of cement plug show that there is no linear relationship between vibration parameters and the mechanical properties of cement slurry. When the vibration parameter is too low or too high, the increase in strength of the cement paste can be neglected. The optimum combination of vibration parameters obtained from the test is as follows; the vibration frequency of 15 Hz, the vibration time of 6 min, and the amplitude of 3 mm. Compared with the non-vibration sample, the cementitious strength is increased by 51%, the compressive strength by 38% and the tensile strength by 20%.

(2) The microstructure of vibrating and non-vibrating cement samples was comparatively analysed through scanning electron microscope observation and a high-pressure mercury injection experiment. Vibration can make the structure of cement paste more uniform and dense. Compared with the un-vibrated cement sample, the porosity of the cement sample under the optimal vibration parameter combination decreased by 19.16%.

(3) Through sensitivity study, it was observed that the influence of each parameter on the performance of cement paste is as follows: vibration frequency is more significant than amplitude, and amplitude is more significant than vibration time.

(4) The simulation experiment of vibration plugging of abandoned wells was carried out. A cement plug cementing quality tester measured the cementing quality of vibrating and non-vibrating samples. The average cementation ratio between the vibrating plug to the inner surface of the casing is 0.89375. The average cementation rate of non-vibrated samples is 0.70625. The post-vibration cementing ratio is greater than 0.8, and the cementing quality is good. Compared with the non-vibrated sample, the cementation ratio of the vibrated sample increased by 27%.

## Declaration of competing interest

The authors declare that they have no known competing financial interests or personal relationships that could have appeared to influence the work reported in this paper.

## Acknowledgement

The authors wish to acknowledge the Open Foundation of Cooperative Innovation Center of Unconventional Oil and Gas, Yangtze University (Ministry of Education & Hubei Province),(Item No. UOGBX2022-04, UOG2022-26, UOGBX2022-05), the National Natural Science Foundation of China “New method and control mechanism of surface rotary steering drilling” (Item No. 51974035, U1262108, U1762214), the key R&D program of Hubei Province “Development and application of multi-dimensional power integrated drilling tools for intelligent drilling” (Item No. 2020BAB055) for the financial support to this paper.

## References

Akbari, S., Taghavi, S.M., 2021. Fluid experiments on the dump bailing method in the plug and abandonment of oil and gas wells. J. Petrol. Sci. Eng. 205 (6), 108920. https://doi.org/10.1016/j.petrol.2021.108920.

Achang, M., Radonjic, M., 2021. Adding olivine micro particles to Portland cement based wellbore cement slurry as a sacrificial material: a quest for the solution in mitigating corrosion of wellbore cement. Cem. Concr. Compos. 121, 104078. https://doi.org/10.1016/j.cemconcomp.2021.104078.

API, 2019. API Specification 10A for Cements and Materials for Well Cementing, twenty-fifth ed.

ASTM C39/C39M-18, 2018. Standard Test Method for Compressive Strength of Cylindrical Concrete Specimens.

Bois, A.P., Vu, M.H., Noël, K., et al., 2019. Evaluating cement-plug mechanical and hydraulic integrity. SPE Drill. Complet. 34 (2), 92–102. https://doi.org/10.2118/191335-PA.

Bageri, B., Ahmed, A., Jaberi, J.A., et al., 2021. Effect of perlite particles on the properties of oil-well class G cement. J. Petrol. Sci. Eng. 199, 108344. https://doi.org/10.1016/j.petrol.2021.108344.

Cui, K.X., Jiang, G.C., Yang, L.L., et al., 2021. Preparation and properties of magnesium oxysulfate cement and its application as lost circulation materials. Petrol. Sci. 18 (5), 1492–1506. https://doi.org/10.1016/j.petsci.2021.08.002.

Carey, J.W., 2013. Geochemistry of wellbore integrity in $CO_2$ sequestration: portland cement-steel-brine-$CO_2$ interactions. Rev. Mineral. Geochem. 77 (1), 505–539. https://doi.org/10.2138/rmg.2013.77.15.

Cai, Y.X., Liu, Q.F., Yu, L.W., et al., 2021. An experimental and numerical investigation of coarse aggregate settlement in fresh concrete under vibration. Cem. Concr. Compos. 122, 104153. https://doi.org/10.1016/j.cemconcomp.2021.104153.

Delage, P., 2010. A microstructure approach to the sensitivity and compressibility of some Eastern Canada sensitive clays. Geotechnique 60 (5), 353–368. https://doi.org/10.1680/geot.2010.60.5.353.

Ding, S.D., Gao, D.L., Wang, Q., et al., 2007. Effect of pulse vibration treatment on early properties of cement stone. Drill. Prod. Technol 30 (6), 105–107. https://doi.org/10.3969/j.issn.1006-768X.2007.06.035 in Chinese.

Feng, Y.C., Gray, K.E., 2017. Parameters controlling pressure and fracture behaviors in field injectivity tests: a numerical investigation using coupled flow and geomechanics model. Comput. Geotech. 87, 49–61. https://doi.org/10.1016/j.compgeo.2017.02.002.

Feng, Y.C., Li, X.R., Gray, K.E., 2017. Development of a 3D numerical model for quantifying fluid-driven interface debonding of an injector well. Int. J. Greenh. Gas Control 62, 76–90. https://doi.org/10.1016/j.ijggc.2017.04.008.

Gajdos, M., Kristofic, T., Jankovic, S., et al., 2015. Use of plasma-based tool for plug and abandonment. In: SPE Offshore Europe Conference and Exhibition. 8-11 September. Aberdeen, Scotland, UK. https://doi.org/10.2118/175431-MS.

Gao, X.J., Zhang, J.Y., Su, Y., 2019. Influence of vibration-induced segregation on mechanical property and chloride ion permeability of concrete with variable rheological performance. Construct. Build. Mater. 194, 32–41. https://doi.org/10.1016/j.conbuildmat.2018.11.019.

Huang, H.H., Gao, X.J., Wang, H., et al., 2017. Influence of rice husk ash on strength and permeability of ultra-high performance concrete. Construct. Build. Mater. 149, 621–628. https://doi.org/10.1016/j.conbuildmat.2017.05.155.
Han, M.L., Wei, X.L., Zhang, J.C., et al., 2022. Influence of structural damage on evaluation of microscopic pore structure in marine continental transitional shale of the Southern North China Basin: a method based on the low-temperature N2 adsorption experiment. Petrol. Sci. 19, 100–115. https://doi.org/10.1016/j.petsci.2021.10.016.
Jiang, J.W., Li, J., Liu, G.H., et al., 2020. Numerical simulation investigation on fracture debonding failure of cement plug/casing interface in abandoned wells. J. Petrol. Sci. Eng. 192, 107226. https://doi.org/10.1016/j.petrol.2020.107226.
James, S., Boukhelifa, L., 2008. Zonal isolation modeling and measurements-past myths and today's realities. SPE Drill. Complet. 23 (1), 68–75. https://doi.org/10.2118/101310-PA.
Khalifeh, M., Hodne, H., Saasen, A., et al., 2013. Techniques and materials for north sea plug and abandonment operations. In: Paper Presented at the Offshore Technology Conference. May Houston, Texas, USA, pp. 6–9. https://doi.org/10.4043/23915-MS.
Kaiser, M.J., 2017. Rigless well abandonment remediation in the shallow water U.S. Gulf of Mexico. J. Petrol. Sci. Eng. 151, 94–115. https://doi.org/10.1016/j.petrol.2017.01.004.
Kjøller, C., Torsæter, M., Lavrov, A., et al., 2016. Novel experimental/numerical approach to evaluate the permeability of cement-caprock systems. Int. J. Greenh. Gas Control 45, 86–93. https://doi.org/10.1016/j.ijggc.2015.12.017.
Kumar, S., Bera, A., Shah, S.N., 2022. Potential applications of nanomaterials in oil and gas well cementing: current status, challenges and prospects. J. Petrol. Sci. Eng. 213, 110395. https://doi.org/10.1016/j.petrol.2022.110395.
Kong, X.Q., Wang, R.Z., Zhang, T.T., et al., 2022. Effects of graphene oxygen content on durability and microstructure of cement mortar composites. Construct. Build. Mater. 354, 129121. https://doi.org/10.1016/j.conbuildmat.2022.129121.
Lecampiona, B., Bunger, A., Kear, J., et al., 2013. Interface debonding driven by fluid injection in a cased and cemented wellbore: modeling and experiments. Int. J. Greenh. Gas Control 18 (7), 208–223. https://doi.org/10.1016/j.ijggc.2013.07.012.
Lanka, S.T., Moses, N.G.A., Suppiah, R.R., et al., 2022. Physio-chemical interaction of Ethylene-Vinyl Acetate copolymer on bonding ability in the cementing material used for oil and gas well. Petroleum Research 7 (3), 341–349. https://doi.org/10.1016/j.ptlrs.2021.10.003.
Li, H.Y., Liu, Y., Yang, K., et al., 2022. Effects of synthetic CSH-tartaric acid nano-composites on the properties of ordinary Portland cement. Cem. Concr. Compos. 129, 104466. https://doi.org/10.1016/j.cemconcomp.2022.104466.
Li, X.J., Zhang, H.K., Bai, Y.F., et al., 2022. Factor analysis and numerical simulation of rock breaking efficiency of TBM deep rock mass based on orthogonal design. J. Cent. South Univ. 29, 1345–1362. https://doi.org/10.1007/s11771-022-4994-9.
Liu, X.P., Guan, M., Jin, Z.J., et al., 2022. Pore structure evolution of lacustrine organic-rich shale from the second member of the Kongdian formation in the Cangdong Sag, Bohai Bay Basin, China. Petrol. Sci. 19, 459–471. https://doi.org/10.1016/j.petsci.2021.12.010.
Moeinikia, F., Ford, E.P., Lohne, H.P., et al., 2018. Leakage calculator for plugged-and-abandoned wells. SPE Prod. Oper. 33 (4), 790–801. https://doi.org/10.2118/185890-PA.
Ma, J.F., Shu, X., Zheng, S.Z., et al., 2022. Effects of polyurethane–silica nanohybrids as additives on the mechanical performance enhancement of ordinary Portland cement paste. Construct. Build. Mater. 338, 127666. https://doi.org/10.1016/j.conbuildmat.2022.127666.
Obodozie, I.E., Trahan, S.J., Joppe, L.C., 2016. Eliminating sustained casing pressure in well abandonment. In: Offshore Technology Conference Asia. 22-25 March. Kuala Lumpur, Malaysia. https://doi.org/10.4043/26432-MS.
Panesar, D.K., Shindman, B., 2012. The effect of segregation on transport and durability properties of self consolidating concrete. Cement Concr. Res. 42 (2), 252–264. https://doi.org/10.1016/j.cemconres.2011.09.011.
GB/T 50266, 2013. Standard for Test Methods of Engineering Rock Mass in Chinese.
SY/T 6646-2017. Well abandonment and inactive well practices (in Chinese).
SY/T 6592-2016. Procedure for cement evaluation (in Chinese).
Trudel, E., Bizhani, M., Zare, M., et al., 2019. Plug and abandonment practices and trends: a British Columbia perspective. J. Petrol. Sci. Eng. 183, 106417. https://doi.org/10.1016/j.petrol.2019.106417.
Vrålstad, T.S., Arild, F., Erling, O., et al., 2019. Plug & abandonment of offshore wells: ensuring long-term well integrity and cost-efficiency. J. Petrol. Sci. Eng. 173, 478–491. https://doi.org/10.1016/j.petrol.2018.10.049.
Whitehouse, 2021. The United States Unveils a US$2,000bn Infrastructure Plan. https://www.whitehouse.gov/briefing-room/statements-releases/2021/03/31/fact-sheet-the-american-jobs-plan/. (Accessed 2 April 2021).
Walsh, S.D.C., Du Frane, W.L., Mason, H.E., et al., 2013. Permeability of wellbore-cement fractures following degradation by carbonated brine. Rock Mech. Rock Eng. 46, 455–464. https://doi.org/10.1007/s00603-012-0336-9.
Wang, W., Taleghani, A.D., 2014. Three-dimensional analysis of cement sheath integrity around wellbores. J. Petrol. Sci. Eng. 121 (2), 38–51. https://doi.org/10.1016/j.petrol.2014.05.024.
Washburn, E.W., 1921. The dynamics of capillary flow. J. Phys. Rev. Lett. 17 (3), 273–283.
Wang, X.G., Ma, B.G., Fu, H.B., 2010. Interface mechanical property and micro-structure of gradient structural concrete(GSC). J. Build. Mater 13 (1), 100–104. https://doi.org/10.3969/j.issn.1007-9629.2010.01.021 in Chinese.
Xu, Z.S., Li, Z.G., 2021. Numerical method for predicting flow and segregation behaviors of fresh concrete. Cem. Concr. Compos. 123, 104150. https://doi.org/10.1016/j.cemconcomp.2021.104150.
Xiong, G.Q., Wang, C., Zhou, S., et al., 2022. Study on dispersion uniformity and performance improvement of steel fibre reinforced lightweight aggregate concrete by vibrational mixing. Case Stud. Constr. Mater. 16, e01093. https://doi.org/10.1016/j.cscm.2022.e01093.
Xiong, G.Q., Wang, C., Zhou, S., et al., 2019. Preparation of high strength lightweight aggregate concrete with the vibration mixing process. Construct. Build. Mater. 229, 116936. https://doi.org/10.1016/j.conbuildmat.2019.116936.
Yu, F., Zhang, X.M., Liu, X.N., et al., 2014. Calibration and testing of acoustic logging tools used in the evaluation of cement bonding conditions. J. Appl. Acoust. 33 (2), 154–159. https://doi.org/10.11684/j.issn.1000-310X.2014.02.009 (in Chinese).
Zhao, X.F., Guan, Z.C., Shi, Y.C., et al., 2017. Mechanism and calculation method of micro-ring gap generation at cementing interface. J. Chin. Univ. Petrol. (Edition of Nat. Sci.) 41 (5), 94–101.. https://doi.org/10.3969/j.issn.1673-5005.2017.05.011 (in Chinese).
Zhao, J.Q., Hu, M.M., Liu, W.M., et al., 2022. Toughening effects of well-dispersed carboxylated styrene-butadiene latex powders on the properties of oil well cement. Construct. Build. Mater. 340, 127768. https://doi.org/10.1016/j.conbuildmat.2022.127768.
Zheng, Y.Z.Z., Zhou, Y., Huang, X.M., et al., 2022. Study on performance improvement of ultra-high performance concrete by vibration mixing. Construct. Build. Mater. 327, 126823. https://doi.org/10.1016/j.conbuildmat.2022.126823.
Zhang, J.Y., Gao, X.J., Yu, L.C., 2020. Improvement of viscosity-modifying agents on air-void system of vibrated concrete. Construct. Build. Mater. 239, 117843. https://doi.org/10.1016/j.conbuildmat.2019.117843.
Zhao, K.Y., Zhao, L.J., Hou, J.R., et al., 2021. Effect of vibratory mixing on the slump, compressive strength, and density of concrete with the different mix proportions. J. Mater. Res. Technol. 21, 1–23. https://doi.org/10.1016/j.jmrt.2021.10.033.
Zhang, Y.J., Yuan, X.B., Ma, Y.Q., et al., 2022. Sensitivity analysis of thermal-fluid coupling parameters of granite with two fractures. In: Jilin Univ, J. (Ed.), , Earth Sci.52, pp. 1–11. https://doi.org/10.13278/j.cnki.jjuese.20210127 in Chinese.